THE JOURNAL OF PHYSICAL CHEMISTRY B

Article

Gated Electron Transfer of Yeast Iso-1 Cytochrome c on Self-Assembled Monolayer-Coated Electrodes

Jiu-Ju Feng, Daniel H. Murgida, Uwe Kuhlmann, Tillmann Utesch, Maria Andrea Mroginski, Peter Hildebrandt, and Inez M. Weidinger

J. Phys. Chem. B, **2008**, 112 (47), 15202-15211 • DOI: 10.1021/jp8062383 • Publication Date (Web): 01 November 2008

Gated Electron Transfer of Yeast Iso-1 Cytochrome c on Self-Assembled Monolayer-Coated Electrodes

Jiu-Ju Feng,[†] Daniel H. Murgida,[‡] Uwe Kuhlmann,[†] Tillmann Utesch,[†] Maria Andrea Mroginski,[†] Peter Hildebrandt,[†] and Inez M. Weidinger*[,†]

Institut für Chemie, Technische Universität Berlin, Sekr. PC14, Strasse des 17. Juni 135, D-10623 Berlin, Germany, and Departamento de Química Inorgánica, Analítica y Química Física/INQUIMAE, Facultad de Ciencias Exactas y Naturales, Universidad de Buenos Aires, Ciudad Universitaria, Pab. 2, piso 1, C1428EHA Buenos Aires, Argentina

Received: July 15, 2008; Revised Manuscript Received: September 16, 2008

Iso-1 yeast cytochrome c (YCC) was adsorbed on Ag electrodes coated with self-assembled monolayers (SAMs) consisting either of 11-mercaptoundecanoic acid (MUA) or of 1:1 mixtures of MUA and either 11-mercaptoundecanol (MU) or 7-mercaptoheptanol (MH). The redox potentials and the apparent rate constants for the interfacial redox process as well as for the protein reorientation were determined by stationary surface-enhanced resonance Raman (SERR) and time-resolved SERR spectroscopy, respectively. For YCC immobilized on MUA and MUA/MU at pH 7.0 and 6.0, the negative shifts of the redox potentials with respect to that for the protein in solution can be rationalized in terms of the potential of the zero-charge determined by impedance measurements. The apparent electron transfer rate constants of YCC on MUA/MU and MU/MH at pH 6.0 were determined to be 8 and 18 s^{-1}, respectively. A decrease of the relaxations constants by a factor of ca. 2 was found for pH 7.0, and a comparable low value was determined for a pure MUA even at pH 6.0. In each system, the rate constant for protein reorientation was found to be the same as that for the electron transfer, implying that protein reorientation is the rate limiting step for the interfacial redox process. This gating step is distinctly slower than that for horse heart cytochrome c (HHCC) observed previously under similar conditions (Murgida, D. H.; Hildebrandt, P. *J. Am. Chem. Soc.* **2001**, *123*, 4062−4068). The different rate constants of protein reorientation for both proteins and the variations of the rate constants for the different SAMs and pH are attributed to the electric field dependence of the free energy of activation which is assumed to be proportional to the product of the electric field strength and the molecular dipole moment of the protein. The latter quantity is determined by molecular dynamics simulations and electrostatic calculations to be more than 2 times larger for YCC than for HHCC. Moreover, the dipole moment vector and the heme plane constitute an angle of ca. 10 and 45° in YCC and HHCC, respectively. The different magnitudes and directions of the dipole moments as well as the different electric field strengths at the various SAM/protein interfaces allow for a qualitative description of the protein-, SAM-, and electrode-specific kinetics of the interfacial redox processes studied in this and previous works.

Introduction

Elucidating the dynamics and mechanism of biological electron transfer (ET) reactions is of particular interest for understanding the function of redox proteins both in their natural environment and in artificial devices of potential technological importance. Thus, immobilization of redox proteins on metal electrodes is essential for developments in molecular electronics, biosensors, and biocatalysis[1−4] Various strategies have been developed to design efficient bioelectronic devices guided by the criteria of high protein loads, good electronic coupling between the immobilized protein and the conductive support, and a sufficient long-term stability. In general, a biocompatible coating of the metal has been found to be essential to avoid protein denaturation and to allow for reversible and fast redox processes. Furthermore, biocompatible coated metal electrodes have been suggested to represent simple but instructive biomimetic systems for biological membranes where most of the redox proteins exert their natural functions.[5−8]

Up to now, a large body of experimental data has been accumulated on the characterization of the interfacial ET processes of redox proteins.[9−18] A common feature of the various systems appears to be that the ET process proceeds in two regimes, the electron tunneling and the gated regime.[19−22] Both mechanisms have been studied in detail on Au and Ag electrodes coated with self-assembled monolayers (SAMs) of ω-functionalized mercaptoalkanes.[23−28] In these studies it has been found that for long alkyl chain lengths (with 10 and more methylene groups) ET is controlled by tunneling whereas for shorter chains electron transfer is gated and essentially distance-independent. Compelling evidence has been recently provided that, at least, for horse heart cytochrome c (HHCC), the gating process is essentially a reorientation of the immobilized protein which takes place with an electric-field depending rate.[24] However, the details of these processes may be different for the various proteins and electrochemical systems since the absolute ET rates in both regimes as well as the onset of the distance-independent region may vary with the protein, the

* To whom correspondence should be addressed. Phone: +49(0)30-31422780. Fax: +49(0)30-31421122. E-mail: i.weidinger@mailbox.tu-berlin.de.
[†] Technische Universität Berlin.
[‡] Universidad de Buenos Aires.

10.1021/jp8062383 CCC: $40.75
Published on Web 11/01/2008

coating, and the metallic support.[25,29,30] Such differences may even refer to related redox proteins such as cytochrome c from horse heart and from yeast (iso-1, YCC). ET of YCC adsorbed on SAMs of carboxyl-terminated mercaptanes is generally slower than that of HHCC under similar conditions[31] but it can be accelerated by using mixed SAMs of carboxyl- and hydroxyl-terminated mercaptanes.[11] These findings were obtained by cyclic voltammetry, which are suitable to determine rate constants of the redox process of the immobilized protein but do not provide information about the underlying molecular processes.

This drawback can be overcome by surface-enhanced resonance Raman (SERR) spectroscopy which allows determining potential structural changes of the heme site while probing the thermodynamics and dynamics of the interfacial redox process.[19,24,32−34] Specifically, SERR spectroscopy can be employed to probe the kinetics of ET and protein reorientation and thus promises to contribute to a comprehensive picture about the parameters that govern the interfacial redox process.[35]

In this work, this method is employed to YCC immobilized on Ag electrodes coated with SAMs of various ω-functionalized mercaptoalkanes. Specifically, this study is directed to elucidate differences and similarities compared to related heme proteins such as HHCC.

Materials and Methods

Materials. Iso-1 yeast cytochrome c from *Saccharomyces cerevisiae* was purchased by Sigma (Steinheim, Germany) and purified by high performance liquid chromatography. 11-mercapto-1-undecanoic acid (MUA), 7-mercapto-1-heptanol (MH), and 11-mercapto-1-undecanol (MU) were purchased from Aldrich (Taufkirchen, Germany). Potassium hydrogen phosphate, potassium dihydrogen phosphate, and potassium sulfate were provided by Merck (Darmstadt, Germany). All solutions were prepared with 18 MΩ Millipore water (Eschborn, Germany). Silver ring electrodes were machined from 99.99% Ag rods (GoodFellow, U.K.).

Surface-Enhanced Resonance Raman Spectroscopy. SERR measurements were carried out with excitation laser of Kr^+ 413 nm and Ar^+ 514 nm (Innova 300, Coherent) using a confocal Raman microscope (LabRam HR-800, Jobin Yvon) equipped with a N_2(l)-cooled back-illuminated charge-coupled device (CCD) detector. The laser beam was focused on the surface of the working electrode with a long working distance objective (20×; numerical aperture 0.35). SERR spectra with 413 nm excitation were acquired with a spectral resolution of 2 cm^{-1} and an increment per data point of 0.57 cm^{-1} using a laser power of ca. 2.5 mW. For 514 nm excitation, the spectral resolution, the increment per pixel and the laser power was 1.6 cm^{-1}, 0.47 cm^{-1}, and ca. 10 mW, respectively. The accumulation times were between 3 and 5 s. All spectra shown in this paper are normalized to the power of 2.5 mW and accumulation time of 5 s. For time-resolved (TR) SERR experiments, potential jumps of variable duration and size were applied to trigger the redox reaction. The relaxation process was probed by measuring the SERR spectra at variable delay time (δ') after each jump. Synchronization of potential jumps and measuring laser pulses was achieved with a homemade four-channel pulse-delay generator. The probe laser pulses were generated by passing the continuous wave laser beam through two consecutive laser intensity modulators (Linos) to afford a total extinction better than 1:25 000 and a time response of ca. 20 ns. The real spectra acquisition time, corresponding to the product of the measuring laser pulse length (Δt) and the number of cycles, was 3−5 s. The time-dependent spectroscopic results are displayed as a function of the delay time (δ) defined as $\delta = \delta' + \Delta t/2$. The working electrode was rotated at ca. 5 Hz to avoid laser-induced sample degradation. After polynomial baseline subtraction, the measured SERR spectra were treated with homemade component analysis software.

Electrode Preparation. The working electrode (Ag ring, 8 mm in diameter, 2.5 mm high) was mechanically polished and electrochemically roughened to produce a SERR active surface following published procedures with minor modification.[36,37] Subsequently, it was immersed in ethanolic solutions of 1 mM MUA or 1:1 mixtures of MUA/MH and MUA/MU (1 mM each) for 24 h to form stable SAMs. After gently washing with ethanol, the SAM-coated electrode was immersed in pure ethanol for 2 h and finally dried with nitrogen. YCC was electrostatically adsorbed to the coated electrodes as follows: the modified electrodes were mounted in an electrochemical cell containing 0.2 μM YCC in the supporting electrolyte and incubated at −500 mV for 30 min before recording the SERR spectra. The supporting electrolyte contained 12.5 mM potassium phosphate and 12.5 mM K_2SO_4 with different pH values by adjusting the ratio of potassium hydrogen phosphate with potassium dihydrogen phosphate. The cell was equipped with a Pt wire as counter electrode and Ag/AgCl (3 M KCl) as reference electrode. Electrode potentials were controlled with an EG&G potentiostat (Princeton Applied Research). All of the experiments were repeated several times to ensure reproducibility.

Electrochemical Impedance Measurements. Electrochemical impedance measurements were performed on a CH instrument electrochemical analyzer 618B (CH Instrument Corp. U.S.A.) under steady-state conditions using an electrochemical cell similar to that used for Raman measurements. The impedance spectra were recorded under various applied potential with AC voltage of 5.0 mV amplitude and in the frequency range of $0.1-10^5$ Hz.

Molecular Dynamics Simulations and Dipole Moment Calculations. Molecular dynamics (MD) simulations combined with dipole moment calculations were performed with the NAMD[38] and CHARMM32[39] packages using the CHARMM27[40] force field for the protein. The force field parameters of the reduced and oxidized heme cofactor were previously optimized by Authenrieth and co-workers.[41] The MD models were based on the crystal structures of YCC deposited in the Protein Data Bank (1YCC[42] and 2YCC[43] for the reduced and oxidized forms, respectively), whereas for HHCC the high resolution ^{1}H NMR solution structures were considered (1OCD[44] and 2FRC[44] for the oxidized and reduced forms, respectively). Missing hydrogen atoms were incorporated to the structures by means of the HBUILD routine.[45] The charges of ionisable groups were set appropriate for pH 7.0 assuming standard pK_a values. On the basis of visual inspection of the environment surrounding the histidines, all histidine residues in YCC and HHCC were protonated on the δ nitrogen atom, except for His26 in YCC which was protonated at the ε nitrogen atom. The total charges of the two proteins yield +8 e in the oxidized form and +7 e in the reduced form. Afterward the protein was solvated in a cubic box of TIP3P water molecules[46] with a volume of 60^3 Å^3. No counterions were added to neutralize the systems. The MD simulations were carried out under periodic boundary conditions with extended electrostatics using the particle-mesh Ewald summation and a cut off distance of 12 Å for the van der Waals interactions. In order to use a 2 fs time step, all bond lengths between heavy atoms and hydrogens were constrained to their minimum energy values by applying the SHAKE algorithm.[47] The energy of the system was initially

minimized with the conjugated gradient integrator using decreasing harmonic constraints on the protein backbone and heme residue (50 kcal/mol Å^2 to 0 kcal/mol Å^2). After 30 ps heating to 300 K using Langevin dynamics,[48] the entire system was equilibrated. During the 310 ps equilibration run, the harmonic constraints on the protein backbone were gradually released. Finally the dynamics of the system was simulated over 1 ns under constant pressure and temperature (NPT ensemble) using the Langevin Piston[48] method.

The permanent electric dipole moments of the two cytochome c proteins in their oxidized and reduced forms were computed using the CHARMM32[39] code. To analyze the fluctuations of dipole moment during the dynamical simulation, time-dependent structures were saved along the simulation every 1 ps, giving 1000 instantaneous structures of protein. The dipole moment of the protein was then computed for each instantaneous structure after centring the protein at the center of mass

Electrostatic potentials were computed using APBS code (http://agave.wustl.edu/apbs), an open source software for the numerical solution of the Poisson−Boltzmann partial differential equation in combination with the VMD1.8.5 visualization software.[49]

Results

SERR Spectra of the Immobilized YCC. YCC was adsorbed onto Ag-electrodes coated with MUA, MUA/MU, and MUA/MH. In all cases, the immobilized YCC displayed high-quality SERR spectra. Adsorption was found to be electrostatic in nature since the immobilized protein could be removed by treatment in concentrated (1 M) KCl solution. Upon Soret-band excitation (413 nm), the SERR spectra are dominated by modes that are known to be characteristic markers for the oxidation, spin, and coordination state (1300−1700 cm^{-1}).[19,20,50] Therefore, this spectral region is particularly appropriate for analyzing the potential-dependent distribution of the oxidized and reduced form of YCC and to detect possible conformational changes that affect the heme site.

To determine the relative contributions of the individual species quantitatively, component analysis was employed that simulates the experimental spectra by weighted superposition of the spectra of the individual species involved.[51] For each experimental spectrum, the analysis yields the spectral amplitudes of these species which are proportional to the relative concentrations. The proportionality factors are determined by comparison of the RR spectra of the oxidized and reduced forms of YCC in solution. These spectra also serve as a starting point for determining the SERR component spectra which were iteratively refined in a global analysis. For all coatings, the stationary potential-dependent SERR spectra, measured from +0.10 to −0.50 V, could be well described solely on the basis of the component spectra of the reduced and oxidized YCC (Figure 1).

Redox Potentials of the Immobilized YCC. The Nernstian plots derived from the component analysis display ideal behavior for a one electron transfer processes with good linear correlations (Figure 2). The redox potential ($E°$) of the adsorbed YCC shows a shift compared to the protein in solution (E^s). For the latter, a value of 82 mV was determined (not shown), which is in good agreement with literature data.[52−54] The redox potentials obtained from the SERR spectroscopic measurements for YCC adsorbed at different SAMs are listed in Table 1. At pH 6.0, the $E°$ values were found to decrease in the following order:

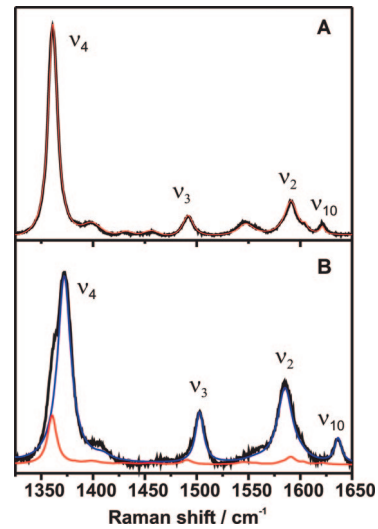

Figure 1. SERR spectra measured with 413 nm excitation of YCC adsorbed on MUA-coated Ag electrode at pH 7.0 buffer at two different electrode potentials: (A) −0.1 V and (B) +0.1 V. The experimental spectra are represented by the black lines, the component spectra of the reduced and oxidized forms are given by the red and blue lines, respectively. YCC oxidized (blue), YCC reduced (red).

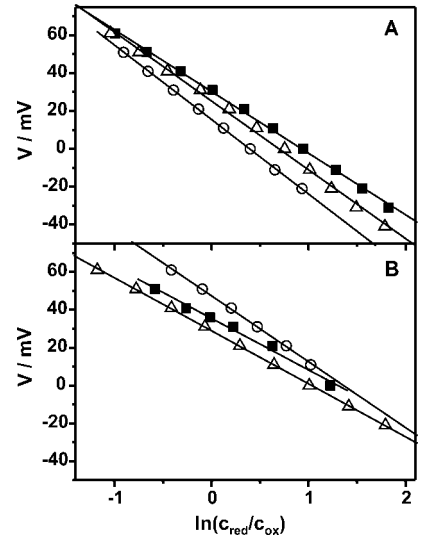

Figure 2. Nernstian plots of the relative concentrations of reduced and oxidized YCC adsorbed on MUA-(solid squares), MUA/MU-(open circles), and MUA/MH-(open triangles) coated Ag electrodes at pH 7.0 (A) and pH 6.0 (B), respectively. The data were obtained from the SERR spectra measured with 413 nm excitation as described in the text.

MUA/MU > MUA > MUA/MH. At each SAM, the redox potentials were slightly more positive at pH 6.0 as compared to pH 7.0.

Potential-Dependent Orientation Changes of the Immobilized YCC. In a first approximation, the heme cofactor of YCC can be considered to be of D_{4h} symmetry.[55,56] Because of the properties of the scattering tensor, totally symmetric (A_{1g}) and nontotally symmetric modes (B_{1g}, B_{2g}, A_{2g}) display a different surface enhancement of the Raman scattering under preresonant excitation (e.g., 514 nm), depending on the orientation of the heme with respect to the metal surface[35] Thus, the variation of the intensity ratio of modes of different symmetry, i.e., A_{1g} versus B_{1g}, are indicative for changes of the orientation of the heme and hence of the immobilized YCC with respect to the surface. These effects can be observed specifically for

TABLE 1: Thermodynamic and Kinetic Parameters of YCC Adsorbed on SAM-Coated Ag Electrodes[a]

SAMs	pH	E_{PZC}/mV	$E°$/mV	$\Delta E_{PZC}°$/mV	E_{RC}/mV	k_{orient} /s^{-1}	k_{redox} /s^{-1}	$I(\nu_{10}/\nu_4)$[b]
MUA	6.0	−350	34	384	−48	5.0	5.2	0.2
	7.0	−450	16	466	−66	n.d.	n.d.	0.8
MUA/MU	6.0	−350	45	395	−37	8.1	7.5	0.6
	7.0	−380	30	410	−52	5.0	4.8	0.6
MUA/MH	6.0	−280	29	309	−52	17.8.	18.0	1.5
	7.0	−350	24	374	−57	9.3	8.6	1.2
solution	7.0		82					5.6

[a] E_{PZC}: Potential of zero charge derived from capacitance measurements. $E°$: Redox potential versus Ag/AgCl. $\Delta E_{PZC}°$: Difference between $E°$ and E_{PZC}. E_{RC}: Redox shift $|E° - E^{s}|$. k_{orient}: Rate constant for protein reorientation for jumps from $E_i = +80$ mV to $E_f = -20$ mV. k_{redox}: Apparent redox rate constant for jumps to $E_f = E°$. [b] Intensity ratio ν_{10}/ν_4 measured at 50 mV.

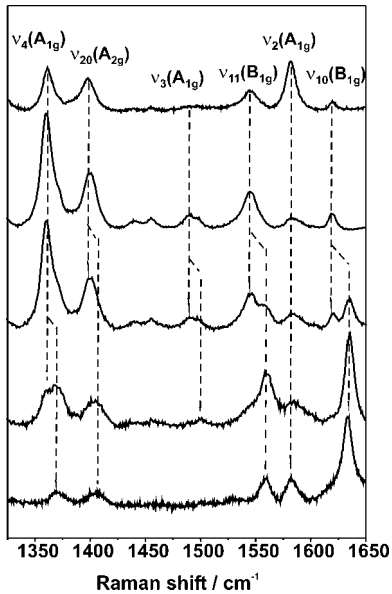

Figure 3. RR and SERR spectra of YCC obtained with 514 nm excitation.. From top to bottom: RR of ferrous YCC; SERR of YCC adsorbed on MUA/MH in pH 7.0 buffer at −400, +50, and +120 mV; RR of ferric YCC. Band assignments followed ref 50.

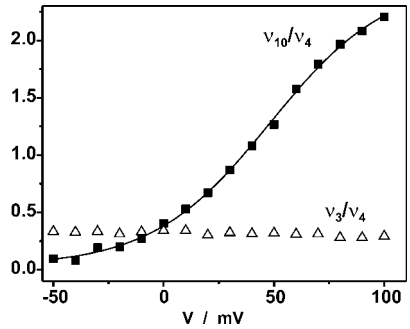

Figure 4. Intensity ratio of $\nu_{10}(B_{1g})/\nu_4(A_{1g})$ (solid squares) and $\nu_3(A_{1g})/\nu_4(A_{1g})$ (open triangles) as a function of electrode potential for YCC adsorbed on a MUA/MH monolayer.

the oxidized form of YCC, monitoring the changes of the $\nu_{10}(B_{1g})/\nu_4(A_{1g})$ intensity ratio as it is shown in Figure 3. As shown in Figure 4, the intensity ratio $\nu_{10}(B_{1g})/\nu_4(A_{1g})$ of oxidized YCC increases with increasing potential, whereas the intensity ratios of the $\nu_3(A_{1g})/\nu_4(A_{1g})$ modes, which are of the same symmetry, remain unchanged. The intensity ratio $\nu_{10}(B_{1g})/\nu_4(A_{1g})$ of adsorbed protein is lower compared to its value in solution (see Table 1). Also slight differences were observed for different monolayer coatings most remarkably for the MUA/MH coating indicating a different orientational distribution Γ_{orient} of YCC on this monolayer.

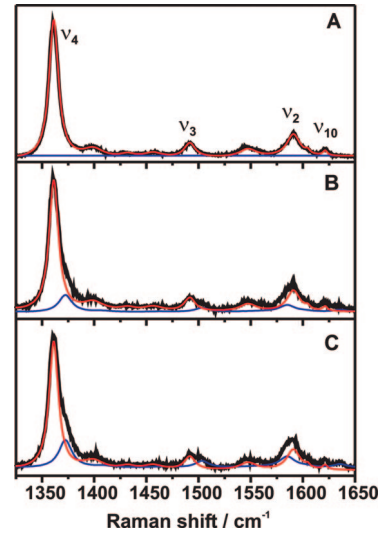

Figure 5. TR-SERR spectra of YCC (413 nm excitation) adsorbed on a MUA/MH-coated Ag electrode at pH 7.0 at different delay times δ after a potential jump from $E_i = -65$ mV to $E_f = +45$ mV: (A) $\delta = 0$ ms; (B) $\delta = 99$ ms (C) $\delta = \infty$. Experimental spectra are given by the black lines while the component spectra of the oxidized YCC and reduced YCC are represented by the blue and red lines, respectively.

The Electron Transfer Dynamics of Immobilized YCC. Time-resolved (TR) SERR spectroscopy was employed to probe the dynamics of the interfacial redox process of the adsorbed YCC using MUA-, MUA/MU-, and MUA/MH-coatings. The experiments were carried out by monitoring the SERR spectral changes at variable delay times (δ) after a potential jump from an initial potential E_i to a final potential E_f. TR-SERR spectra were recorded with Soret- and Q-band (514 nm) excitation and quantitatively analyzed as described above.

For experiments with 413 nm excitation, the final potential was set equal to the redox potential ($E_f = E°$) such that the electron transfer processes were controlled by a driving force of 0 eV. The initial potential was chosen to be 100 mV more negative than $E°$. Thus, YCC is largely reduced at E_i such that the spectral changes resulting from potential jumps to E_f are relatively pronounced and can easily be followed. Representative TR SERR spectra of YCC adsorbed on a MUA/MH-coated electrode are shown in Figure 5.

Since probing the time-dependent changes of protein orientation (514 nm excitation) is restricted to the ferric state, the potential range spanned by E_i and E_f must be more positive than in the case of 413 nm excitation. For the majority of experiments E_i and E_f were chosen to be 80 and −20 mV, respectively. However, under these conditions, the TR SERR experiments of YCC adsorbed on MUA-coated Ag electrodes at pH 7.0 reveal a steady increase of oxidation which evidently

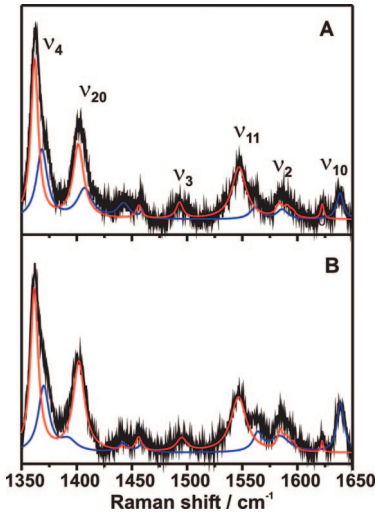

Figure 6. TR-SERR spectra of YCC (514 nm excitation) adsorbed on a MUA/MH-coated Ag electrode at pH 7.0 at different delay times δ after a potential jump from $E_i = +41$ mV to $E_f = +81$ mV: (A) $\delta = 41$ ms; (B) $\delta = 710$ ms. Experimental spectra are given by the black lines while the component spectra of the oxidized YCC and reduced YCC are represented by the blue and red lines, respectively.

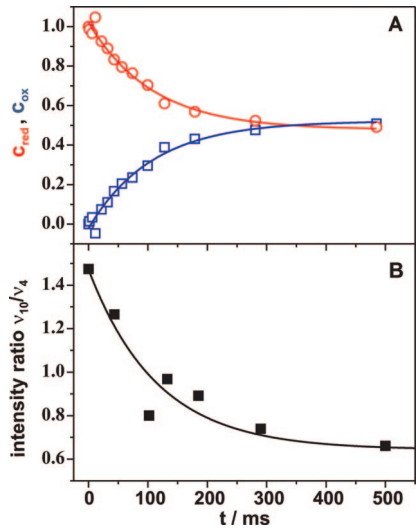

Figure 7. (A) Time-dependent changes of the relative concentrations of the reduced (red circles) and oxidized (blue squares) YCC, obtained from TR SERR spectra measured at 413 nm. (B) Time-dependent changes of the intensity ratio $\nu_{10}(B_{1g})/\nu_4(A_{1g})$, obtained from TR SER spectra measured at 514 nm. All TR SER(R) spectra were obtained from YCC adsorbed on a MUA/MH-coated Ag electrode at pH 7.0.

occurs on the time scale of minutes (Figure 8). The stationary SERR spectra measured before and after TR experiments display upshifts of both the ν_{10} mode from 1637 to 1640 cm^{-1} and of the ν_4 mode from 1370 to 1374 cm^{-1}. These upshifts are characteristic of the formation of the conformational state B2 in which the native Met80 ligand of the heme is replaced by a histidine.[57] This transition is associated with a large negative shift of the redox potential to ca. −350 mV. Thus, during TR SERR experiments, subsequent to the relatively fast electron transfer of the reduced B1, a fraction of the oxidized B1 is slowly converted to the oxidized B2 during the dwell time at positive potentials (80 mV). After the potential jump back to −20 mV, only the oxidized B1 species is reduced whereas the B2 state remains oxidized. As a result, the repetitive potential jumps from −20 to +80 mV lead to a steady accumulation of the oxidized B2 which under the conditions of these experiments

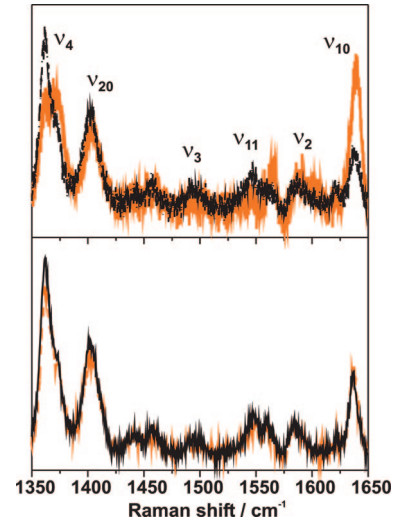

Figure 8. Comparison of SER spectra (514 nm excitation) of YCC before (black) and after (orange) time-dependent SER measurements. Spectra in (A) and (B) refer to YCC adsorbed on MUA- and MUA/MH-coated Ag electrodes at pH 7.0.

is irreversible. These findings also provide an explanation for the results of previous electrochemical studies on YCC on MUA-coated Au electrodes.[31] In these studies, more than one redox transition was observed in the cyclic voltammograms at pH 7.0, thereby prohibiting the determination of the electron transfer rate constant.

In contrast to YCC on MUA-coated Ag electrodes at pH 7.0., lowering the pH to 6.0 as well as using mixed coatings, a fully reversible behavior was observed at both pH and the TR SERR spectra could be well described solely using the component spectra of the reduced and oxidized B1 without any interference of the B2 state (Figure 6). Thus, the kinetic data derived from TR-SERR spectra could be analyzed on the basis of a one-step relaxation process (Figure 7), allowing for the determination of the relaxation constants k_{redox} and k_{orient} for the redox transition (413 nm) and protein reorientation (514 nm), respectively (Table 1).

In general, we note that for a given coating and pH the values for k_{redox} and k_{orient} are essentially the same within the experimental accuracy. Furthermore, the relaxation constants decrease in the order MUA < MUA/MU < MUA/MH and from pH 6.0 to pH 7.0. In each case, the values are distinctly lower than that determined for HHCC immobilized on MUA-coated Ag electrodes (86 s^{-1} at pH 7.0).[58]

Zero Charge Potential Determination. On the basis of the method proposed by Kolb et al.,[59,60] electrochemical impedance experiments were performed at various potential and SAM components. From the plots of the capacitance versus potential, the potential of zero charge (E_{PZC}) for Ag modified with MUA-, MUA/MU-, and MUA/MH-coatings was estimated. As shown in Table 1, E_{PZC} increases distinctly for all coatings compared to the value obtained at a bare Ag electrode (−0.97 V).[61] In agreement with data published previously for thiol-based-SAM modified Au electrodes,[62] we observe generally a larger increase of E_{PZC} at pH 6 compared to pH 7 and for SAMs containing hydroxyl-groups. The largest increase was measured for MUA/MH coatings at pH 6 were a shift of 0.69 V compared to bare Ag was observed.

Molecular Dynamics Simulations and Dipole Moment Calculations. The two solution NMR average structures of the oxidized and reduced forms of HHCC deviate significantly from each other.[44] The all-residues root-mean-square deviation about

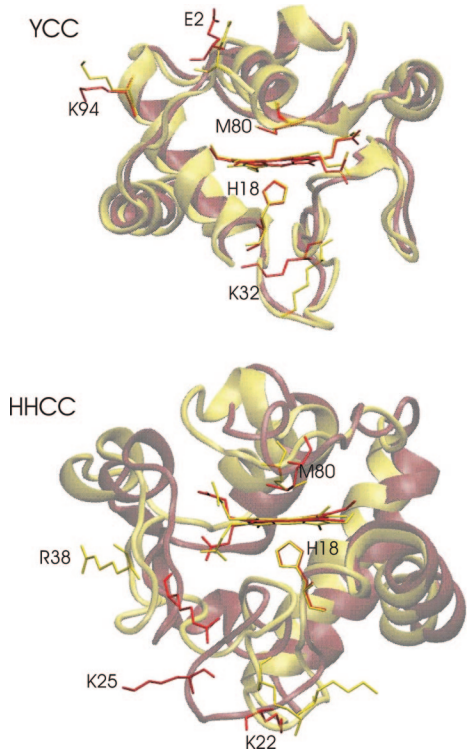

Figure 9. Average structures of the reduced (red) and oxidized (yellow) forms of YCC and HHCC obtained from 1 ns MD simulation.

the average structure is 5.56 Å (9.96 Å) for the backbone (all heavy atoms). The structural differences between the average structure obtained from the MD trajectories are distinctly smaller (Figure 9). For this case, the all-residues root-mean-square deviation about the average structure is reduced to 2.89 Å (3.95 Å) for the backbone (all heavy atoms). The major structural differences are noted at the long random coil fragments between residues 20 and 29 (Figure 9). This loop contains the Lys resides 25 and 22 with their positively charged amino groups being displaced by ca. 15 Å in the oxidized structure compared to the reduced one. Furthermore, there are changes of the secondary structure such as the disappearance of the α-helix between residues 70 and 76 and the formation of a β-sheet between residues 34 and 41 in the reduced form. The latter structural change is associated with the movement of Arg38 toward the solvent. No important structural changes are observed at the heme or in its immediate environment. The coordination of Met80 and His18 to the Fe is not significantly altered by changes in the oxidation state of the heme. However, upon comparing the two predicted average geometries, we note a rotation of Met80, which may be responsible for the changes of the secondary structure of neighboring residues.

In contrast to HHCC, there are no significant structural differences between the crystallographic structures of the reduced and the oxidized forms of YCC. The all-residues root-mean-square deviation about the average structure is 0.19 Å for the backbone. The average structures obtained from the MD simulation deviate only slightly from the corresponding X-ray structures. For the oxidized and reduced forms of YCC the rmsd is only 0.63 Å (3.13 Å) and 0.66 Å (3.16 Å) for the backbone (all heavy atoms), respectively. There are also only negligible differences between the MD average structures for the two oxidation states with a rmsd of the average structure 0.3 Å (0.59 C) for the backbone (for all heavy atoms). This result indicates that, also for YCC, the oxidation of the heme has no relevant effect on the protein structure. A closer look in the heme binding

TABLE 2: Dipole Moments (D) of YCC and HHCC in the Reduced and Oxidized States[a]

	YCC			HHCC		
	red	ox	red -ox	red	ox	red - ox
static						
X-ray /NMR structure	506	561	55	275	168	−107
MD						
average	536	544	8	150	184	34
minimum	465	452		80	103	
maximum	602	607		224	280	
distribution bandwidth	53	46		50	55	

[a] Structural data of reduced YCC, oxidized YCC, reduced HHCC, and oxidized HHCC were taken from PDB files 1YCC, 2YCC, 1OCD, and 2FRC, respectively.

pocket shows that the positions of the Met80 and His18 are essentially unaltered (Figure 9). The largest structural difference between the average structures of the two oxidation states is observed at the C-terminus where the propionic side chains of Glu2 are displaced by ca. 8 Å from each other.

The average dipole moment obtained from the instantaneous structures along the 1 ns MD simulations is more than two times larger for YCC than for HHCC (Table 2). The results are in agreement with previous calculations by Koppenol et al.[63] For YCC, these authors obtained a very similar dipole moment (522 D for the ferrous state), whereas the value for HHCC (299 D for the ferrous state) was overestimated compared to the present results. The large difference in dipole moment of these two species can be explained in terms of the protein shape and charge distribution. Figure 10 shows the calculated electrostatic potentials for reduced YCC and HHCC. In HHCC, the protein adopts a more globular shape and the charge is more uniformly distributed on the surface. YCC, on the other hand, exhibit a slightly more elongated form with positively and negatively charged patches on opposite sides of the ellipsoid.

Furthermore, the orientation of the dipole moments with respect to the heme cofactor is different in the two cytochrome species. In YCC, the dipole moment vector forms an angle of ca. 10° with respect to the porphyrin plane whereas in HHCC this angle increases to ca. 45° angle (Figure 10). For both proteins, the dipole moment is slightly larger for the oxidized than for the reduced form. This is not the case when the dipole moments of HHCC are calculated using static solution NMR structures. Then the dipole moment of the reduced form is strongly overestimated such that it becomes distinctly larger than that of the oxidized form. More reliable values are certainly obtained upon averaging over a long MD simulation.

The thermal fluctuations of the dipole moments were further investigated by analyzing the statistical distribution of the modulus of the dipole moment vectors along the 1 ns MD simulation (Figure 11). All distribution plots could be equally well fitted with Gaussian functions with bandwidth of ca. 50 D. This result indicates that changes in the dipole moment of up to 50 D can be expected as a result of thermal fluctuations of the protein. In YCC, for example, the small difference between the dipole moment of the oxidized and the reduced forms of 8 D results most probably from slight changes in the orientation of the amino acid side chains, in particular Glu2 (vide supra) and Lys94 and Lys32. This small dipole moment difference cannot be related with changes in the oxidation state of the heme, since it lies within the thermal fluctuation of the system. This conclusion is also true for HHCC, although the dipole moment difference between reduced and oxidized forms is predicted to be larger than for YCC.

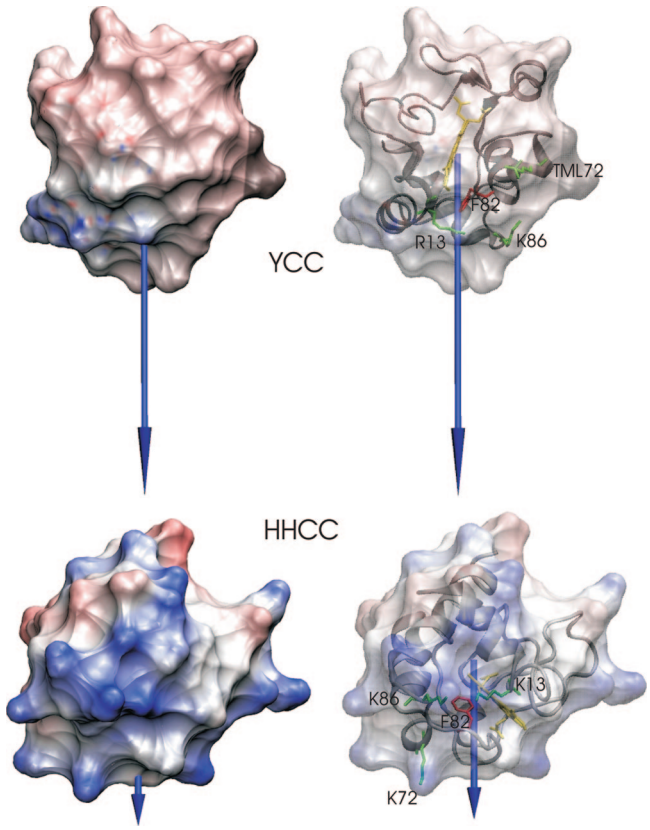

Figure 10. Calculated electrostatic potentials and electric dipole moments of reduced YCC and reduced HHCC (left). Orientation of the calculated dipole moments with respect to the heme plane in both structures (right).

Discussion

Redox Potential Shift. It has been shown previously that HHCC displays a negative shift of the redox potential upon immobilization to Ag electrodes coated with carboxylate-terminated SAMs.[64] This shift $E_{RC} = |E^O - E^s|$ is attributed to the interfacial potential drop which mainly depends on the charge distribution and density in the SAM/HHCC interface. For HHCC adsorbed on MUA-coated electrodes at pH 7.0, E_{RC} was determined to be −41 mV, whereas a larger negative shift (−66 mV) is observed in the present work for YCC under otherwise identical conditions. This difference in attributed to the different charge distribution on the surface of both proteins which in turn is reflected by the quite different dipole moments of YCC and HHCC. Lowering the pH to 6.0 is expected to cause a decrease of the charge density on the SAM surface and thus of the magnitude of the redox potential shift which is in fact observed (−48 mV).

In mixed MUA/MU monolayers, there are two opposing effects on the surface charge density since the reduction of carboxylic head groups by a factor of 2 lowers the number of ionizable groups whereas this dilution also causes a decrease of the apparent pK_A corresponding to an increase of the negative surface charge density. As a result, the magnitude of the redox potential shift is only slightly lower than for pure MUA SAMs at both pH 6.0 and 7.0. One may take the difference between the applied potential E and the potential of zero charge $\Delta E_{PZC} = |E - E_{PZC}|$ of the SAM-coated electrodes as a measure for the charge density on the SAM surface and assume this quantity for $E = E°$ to be proportional to E_{RC}.[65] In fact, for MUA and MUA/MU and both pH 6 and 7, the values determined for E_{PZC} by impedance spectroscopy reflect qualitatively the decrease of E_{RC} with decreasing $\Delta E_{PZC}°$. However, for MUA/MH the redox potential shifts are significantly more negative than predicted by the relatively low value of $\Delta E_{PZC}°$ and only slightly depend on the pH. It may be that due to the different chain lengths the actual dilution effect for mixtures of MUA and MH is smaller. The higher values for $\nu_{10}(B_{1g})/\nu_4(A_{1g})$ also suggest a different orientational distribution of YCC for this monolayer, which could result in a smaller distance between the heme and the charged groups of the monolayer. As a consequence the redox potential shifts lie in between those determined for MUA and MUA/MU.

Electron Transfer Processes. The interfacial redox process of HHCC has been shown to involve a complex reaction mechanism including protein reorientation, electron tunneling, and redox-linked structural changes of the protein, which can be selectively monitored by time-resolved SERR and SEIRA spectroscopy.[13,24] The relationship between electron transfer and protein reorientation can be understood on the basis of the strong angular- and distance-dependence of the electronic coupling parameter H_{AB} which governs the electron tunneling rate. Thus, for a given distance H_{AB} sensitively varies with the orientation of the heme relative to the surface. Electrostatic adsorption of HHCC and YCC leads to a distribution of orientations, each of them being associated with different electron tunneling rates.[35] If the transitions between the various orientations are fast, the main reaction channel for the electron transfer process is provided by orientations that exhibit the largest electronic coupling parameter. In the opposite case, ET is controlled by the orientational distribution Γ_{orient} and the reorientation rate constant(s) k_{orient}.

For HHCC immobilized on MUA (pH 7.0), protein reorientation has been found to be distinctly faster than electron tunneling at zero-driving force and the concomitant protein structural changes.[35,66] Redox processes of YCC at these distances reveal a different dynamic behavior. For pure MUA SAMs at pH 6.0 and mixed MUA/MH and MUA/MU SAMs at pH 6.0 and 7.0, the relaxation constants for the redox transitions (k_{redox}) determined with 413 nm excitation are much slower (5−18 s^{-1}) than that obtained for HHCC on a MUA-coated electrode at pH 7.0 (83 s^{-1}).[58] Moreover, for YCC at each SAM coating, the values for k_{redox} are identical to those of the relaxation constants for protein reorientation (k_{orient}) obtained by TR SERR experiments with 514 nm excitation. Again, this behavior is different for HHCC for which (MUA, pH 7.0) k_{orient} was determined to be ca. 380 s^{-1}. These findings imply that, unlike to HHCC, reorientation of the immobilized YCC constitutes the rate-limiting step of the interfacial redox process in each case.

These results can be understood on the basis of the electric field dependence of both the orientational distribution Γ_{orient} and the reorientation rate constant(s) k_{orient}. The latter has been shown to decrease with increasing electric field strength $\vec{E}_F$[35] most likely via an increase of the free energy of activation by a term proportional to $\vec{\mu}\cdot\vec{E}_F$, where $\vec{\mu}$ is the dipole moment of the protein. The electric field strength at the SAM/protein interface is mainly controlled by the interfacial charge distribution and thus is related to the value of ΔE_{PZC} (vide supra). Indeed, the values for k_{orient}, measured for jumps to the respective redox potentials, display an almost linear dependence on $\Delta E_{PZC}°$ with increasing rate constants upon decreasing $\Delta E_{PZC}°$.

Also Γ_{orient} is controlled by the electric field $\vec{E}_F$ and the dipole moment $\vec{\mu}$. In a first approximation, one may assume that immobilized cytochrome will preferentially align with its dipole moment parallel to the electric field vector. On the basis of the

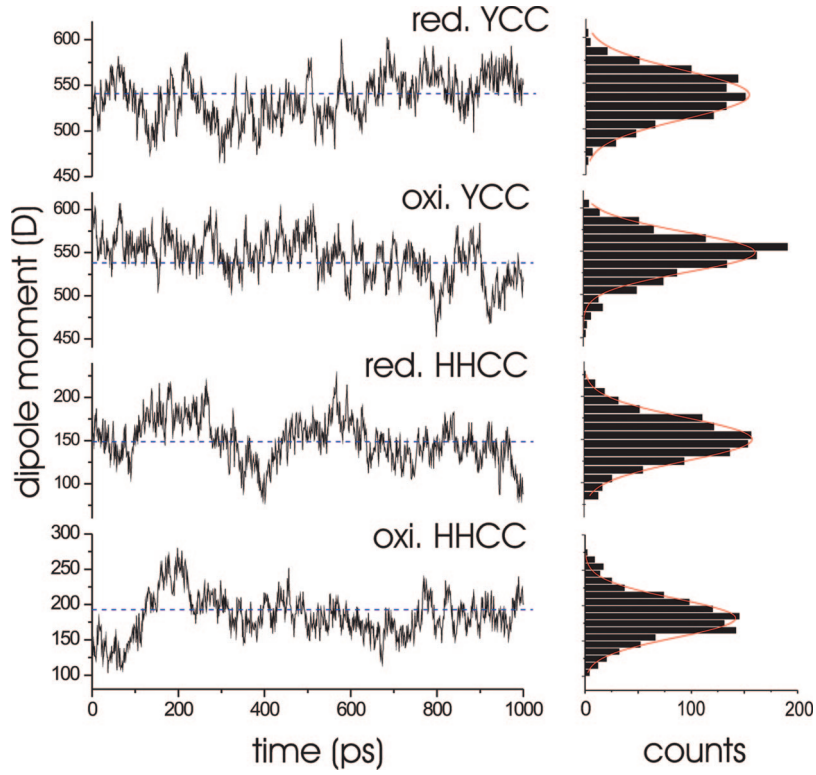

Figure 11. Fluctuations of the calculated dipole moments of YCC and HHCC in the reduced and oxidized forms during the 1 ns MD trajectory (left) and their statistical distributions (right).

present dipole moment calculations and taking into account that the electric field vector is perpendicular to the SAM surface, the most probable orientation would correspond to tilt angle of the heme plane with respect to the surface normal of ca. 10 and 45° for YCC and HHCC, respectively. From this point of view, one would expect a faster electron transfer for YCC proteins compared to HHCC if ET were to occur from the thermodynamically stable configurations of the electrostatic complexes.

It is now interesting to compare the present results with those previously obtained for HHCC on MUA SAMs.[35] Clearly, the drastically lower value of k_{orient} for YCC immobilized on MUA-coated electrodes cannot be related to an increase of the electric field strength but can only be understood in terms of a larger dipole moment of YCC as compared to HHCC. This is in fact confirmed by the calculations in this work. The average dipole moment derived from MD simulations is by ca. 270 D larger for YCC than for HHCC. This quantity would correspond to a difference in activation energy of ca. 50 kJ/mol assuming an electric field strength of 10^8 V/m. Although we do not know how the activation energy depends on the electric field, the substantial decrease of k_{orient} in YCC as compared to HHCC can readily be understood, particularly taking into account that the interfacial electric field strength may be much higher than 10^8 V/m.[64]

The large difference in the molecular dipole moment between both proteins also provides an explanation for the failure to probe the electron transfer process of YCC on MUA at pH 7.0, where electric field strengths are higher than at pH 6.0 (vide supra). In this case, the formation of the conformational state B2 during the TR SERR experiments impaired the analysis of the ET dynamics. Under the same conditions, no formation of B2 is observed for HHCC.[64] The transition from the native state B1 to the conformational state B2 has been shown to depend on the electric field strength and the dipole moment difference between the states B1 and B2,[64] implying that this difference is larger for YCC as compared to HHCC.

Following this interpretation one may readily reconcile the present results and the previous data obtained for YCC on coated Au electrodes.[11] On the basis of CV measurements, k_{redox} was determined to be 500 s^{-1} for a MUA/MU SAM that is ca. 50 times larger than the rate constant obtained in this work for Ag electrodes under otherwise similar conditions. Taking into account that E_{PZC} of MUA- and MU-coated Au electrodes is close to $E°$ of the adsorbed YCC,[62] one may assume a similar value also for Au electrodes with mixed MUA/MU coatings. As a consequence, the electric field at the SAM/protein interface is likely to be much lower than for the respective coated Ag electrodes, leading to a much faster protein reorientation.

Note that for both YCC and HHCC the MD simulations indicate that the fluctuations of the dipole moment due to the protein dynamics are larger than the difference of the average values of the oxidized and reduced forms such that redox-state specific effects of the dipole moment on the interfacial redox process are not very likely.

The differences observed for YCC and HHCC may have implications for the redox processes under physiological conditions. On the basis of the available crystal structures of the reaction partners of cytochrome c,[67,68] it is not straightforward to assess the direction of the electric field that prealigns the cytochrome in the instantaneously formed protein complex. Such a prediction is particularly complicated since the effective electric field is not only based on the charge distribution in the respective partner protein but also on the electrostatic properties of the environment, specifically the transmembrane potential. However, it appears to be unlikely that the optimum orientation of HHCC corresponds to a 45° angle between the heme plane and the effective electric field vector. As a consequence, we conclude that the precursor complex of HHCC is not competent for electron tunneling but a reorientation step is required prior

to ET with either cytochrome c oxidase and cytochrome c reductase. The situation is different for YCC as presumably even lower electric field strengths lead to a strong decrease in its ability to reorient fast enough for efficient ET. Therefore binding to its respective partner enzymes should occur under lower electrostatic conditions and is indeed dominated by hydrophobic and van der Waals interactions.[68,69]

Conclusions

In this work, the redox potential and kinetics of the redox process of YCC adsorbed on Ag electrodes coated with MUA-, MUA/MU-, and MUA/MH-SAMs have been determined. It could be shown that the interfacial redox process of YCC is controlled by the distribution and dynamics of protein orientations, thereby following a similar complex reaction mechanism as in the case of HHCC. However, the electric field dependence of the redox process is different for YCC and HHCC. Unlike HHCC, the interfacial redox process of YCC for each of the SAMs studied in this work is gated by protein reorientation due to its distinctly larger dipole moment that results in a larger activation energy for rotational diffusion. It was demonstrated that the rates for protein reorientation depend on the product of the protein's dipole moment and the interfacial electric field strength, the latter being a function of ΔE_{PZC}. In this respect, lower interfacial electric field strength may be the origin for the much faster redox process observed on MUA/MU-coated Au electrodes.

Acknowledgment. Financial support by Fonds der Chemischen Industrie, the Deutsche Forschungsgemeinschaft (SFB 498), Cluster of Excellence (UniCat), the Volkswagenstiftung (I/80816) and ANPCyT (PICT2006-459) is gratefully acknowledged. We thank Hendrik Naumann for providing analysis software and Dr. Ingo Zebger and Steve Kaminski for critical comments.

References and Notes

(1) Willner, I.; Katz, E. *Bioelectronics*; Wiley-VCH: Weinheim, 2005.
(2) Willner, I.; Katz, E. *Angew. Chem., Int. Ed.* **2000**, *39*, 1180–1218.
(3) Rusmini, F.; Zhong, Z. Y.; Feijen, J. *Biomacromolecules* **2007**, *8*, 1775–1789.
(4) Armstrong, F. A.; Wilson, G. S. *Electrochim. Acta* **2000**, *45*, 2623–2645.
(5) Flink, S.; van Veggel, F. C. J. M.; Reinhoudt, D. N. *Adv. Mater.* **2000**, *12*, 1315–1328.
(6) Katz, E.; Willner, I.; Wang, J. *Electroanal.* **2004**, *16*, 19–44.
(7) Chen, D.; Wang, G.; Li, J. H. *J. Phys. Chem. C* **2007**, *111*, 2351–2367.
(8) Zhang, J.; Chi, Q.; Kuznetsov, A. M.; Hansen, A. G.; Wackerbarth, H.; Christensen, H. E. M.; Andersen, J. E. T.; Ulstrup, J. *J. Phys. Chem. B* **2002**, *106*, 1131–1152.
(9) Armstrong, F. A.; Hill, H. A. O.; Walton, N. J. *Q. Rev. Biophys.* **1985**, *18*, 261–322.
(10) Nahir, T. M.; Clark, R. A.; Bowden, E. F. *Anal. Chem.* **1994**, *66*, 2595–2598.
(11) El Kasmi, A.; Wallace, J. M.; Bowden, E. F.; Binet, S. M.; Linderman, R. J. *J. Am. Chem. Soc.* **1998**, *120*, 225–226.
(12) Armstrong, F. A.; Camba, R.; Heering, H. A.; Hirst, J.; Jeuken, L. J. C.; Jones, A. K.; Leger, C.; Mcevoy, J. P. *Faraday Discuss.* **2000**, 191–203.
(13) Murgida, D. H.; Hildebrandt, P. *Phys. Chem. Chem. Phys.* **2005**, *7*, 3773–3784.
(14) Udit, A. K.; Hill, M. G.; Gray, H. B. *Langmuir* **2006**, *22*, 10854–10857.
(15) Wang, J. *Chem. Rev.* **2008**, *108*, 814–825.
(16) Bortolotti, C. A.; Battistuzzi, G.; Borsari, M.; Facci, P.; Ranieri, A.; Sola, M. *J. Am. Chem. Soc.* **2006**, *128*, 5444–5451.
(17) Bortolotti, C.; Borsari, M.; Sola, M.; Chertkova, R.; Dolgikh, D.; Kotlyar, A.; Facci, P. *J. Phys. Chem. C* **2007**, *111*, 12100–12105.
(18) Heering, H. A.; Wiertz, F. G. M.; Dekker, C.; de Vries, S. *J. Am. Chem. Soc.* **2004**, *126*, 11103–11112.
(19) Murgida, D. H.; Hildebrandt, P. *Acc. Chem. Res.* **2004**, *37*, 854–861.
(20) Murgida, D.; Hildebrandt, P. *Surf. Enhanced Raman Scattering* **2006**, *103*, 313–334.
(21) Jeuken, L. J. C.; Mcevoy, J. P.; Armstrong, F. A. *J. Phys. Chem. B* **2002**, *106*, 2304–2313.
(22) Jeuken, L. J. C. *BBA Bioenergetics* **2003**, *1604*, 67–76.
(23) Tarlov, M. J.; Bowden, E. F. *J. Am. Chem. Soc.* **1991**, *113*, 1847–1849.
(24) Murgida, D. H.; Hildebrandt, P. *Chem. Soc. Rev.* **2008**, *37*, 937–945.
(25) Avila, A.; Gregory, B. W.; Niki, K.; Cotton, T. M. *J. Phys. Chem. B* **2000**, *104*, 2759–2766.
(26) Chi, Q. J.; Zhang, J. D.; Andersen, J. E. T.; Ulstrup, J. *J. Phys. Chem. B* **2001**, *105*, 4669–4679.
(27) Leopold, M. C.; Bowden, E. F. *Langmuir* **2002**, *18*, 2239–2245.
(28) Xu, J. S.; Bowden, E. F. *J. Am. Chem. Soc.* **2006**, *128*, 6813–6822.
(29) Wei, J. J.; Liu, H. Y.; Khoshtariya, D. E.; Yamamoto, H.; Dick, A.; Waldeck, D. H. *Angew. Chem., Int. Ed* **2002**, *41*, 4700–4703.
(30) Yue, H. J.; Khoshtariya, D.; Waldeck, D. H.; Grochol, J.; Hildebrandt, P.; Murgida, D. H. *J. Phys. Chem. B* **2006**, *110*, 19906–19913.
(31) de Groot, M. T.; Merkx, M.; Koper, M. T. M. *Langmuir* **2007**, *23*, 3832–3839.
(32) Siebert, F.; Hildebrandt, P. *Vibrational Spectroscopy in Life Science*; Wiley-VCH: Weinheim, 2008.
(33) Millo, D.; Bonifacio, A.; Ranieri, A.; Borsari, M.; Gooijer, C.; van der Zwan, G. *Langmuir* **2007**, *23*, 9898–9904.
(34) Millo, D.; Bonifacio, A.; Ranieri, A.; Borsari, M.; Gooijer, C.; van der Zwan, G. *Langmuir* **2007**, *23*, 4340–4345.
(35) Kranich, A.; Ly, H. K.; Hildebrandt, P.; Murgida, D. H. *J. Am. Chem. Soc.* **2008**, *130*, 9844–9848.
(36) Millo, D.; Ranieri, A.; Koot, W.; Gooijer, C.; van der Zwan, G. *Anal. Chem.* **2006**, *78*, 5622–5625.
(37) Wackerbarth, H.; Klar, U.; Gunther, W.; Hildebrandt, P. *Appl. Spectrosc.* **1999**, *53*, 283–291.
(38) Phillips, J. C.; Braun, R.; Wang, W.; Gumbart, J.; Tajkhorshid, E.; Villa, E.; Chipot, C.; Skeel, R. D.; Kale, L.; Schulten, K. *J. Comput. Chem.* **2005**, *26*, 1781–1802.
(39) Brooks, B. R.; Bruccoleri, R. E.; Olafson, B. D.; States, D. J.; Swaminathan, S.; Karplus, M. *J. Comput. Chem.* **1983**, *4*, 187–217.
(40) Foloppe, N.; MacKerell, A. D. *J. Comput. Chem.* **2000**, *21*, 86–104.
(41) Autenrieth, F.; Tajkhorshid, E.; Baudry, J.; Luthey-Schulten, Z. *J. Comput. Chem.* **2004**, *25*, 1613–1622.
(42) Louie, G. V.; Brayer, G. D. *J. Mol. Biol.* **1990**, *214*, 527–555.
(43) Berghuis, A. M.; Brayer, G. D. *J. Mol. Biol.* **1992**, *223*, 959–976.
(44) Qi, P. X. R.; Beckman, R. A.; Wand, A. J. *Biochemistry* **1996**, *35*, 12275–12286.
(45) Brunger, A. T.; Karplus, M. *Proteins* **1988**, *4*, 148–156.
(46) Jorgensen, W. L.; Chandrasekhar, J.; Madura, J. D.; Impey, R. W.; Klein, M. L. *J. Chem. Phys.* **1983**, *79*, 926–935.
(47) van Gunsteren, W. F.; Berendsen, H. J. C. *Mol. Phys.* **1977**, *34*, 1311–1327.
(48) Feller, S. E.; Zhang, Y. H.; Pastor, R. W.; Brooks, B. R. *J. Chem. Phys.* **1995**, *103*, 4613–4621.
(49) Humphrey, W.; Dalke, A.; Schulten, K. *J. Mol. Graphics* **1996**, *14*, 33.
(50) Hu, S. Z.; Morris, I. K.; Singh, J. P.; Smith, K. M.; Spiro, T. G. *J. Am. Chem. Soc.* **1993**, *115*, 12446–12458.
(51) Döpner, S.; Hildebrandt, P.; Mauk, A. G.; Lenk, H.; Stempfle, W. *Spectrochim. Acta* **1996**, *A 51*, 573–584.
(52) Rafferty, S. P.; Pearce, L. L.; Barker, P. D.; Guillemette, J. G.; Kay, C. M.; Smith, M.; Mauk, A. G. *Biochemistry* **1990**, *29*, 9365–9369.
(53) Davies, A. M.; Guillemette, J. G.; Smith, M.; Greenwood, C.; Thurgood, A. G. P.; Mauk, A. G.; Moore, G. R. *Biochemistry* **1993**, *32*, 5431–5435.
(54) Ikeshoji, T.; Taniguchi, I.; Hawkridge, F. M. *J. Electroanal. Chem.* **1989**, *270*, 297–308.
(55) Kneipp, K.; Moskovits, M.; Kneipp, H. *Surface-enhanced Raman Scattering*; Springer: Berlin, 2006.
(56) Macdonald, I. D. G.; Smith, W. E. *Langmuir* **1996**, *12*, 706–713.
(57) Wackerbarth, H.; Hildebrandt, P. *ChemPhysChem* **2003**, *4*, 714–724.
(58) Murgida, D. H.; Hildebrandt, P. *J. Am. Chem. Soc.* **2001**, *123*, 4062–4068.
(59) Lipkowski, J.; Stolberg, L.; Yang, D. F.; Pettinger, B.; Mirwald, S.; Henglein, F.; Kolb, D. M. *Electrochim. Acta* **1994**, *39*, 1045–1056.
(60) Pajkossy, T.; Kolb, D. M. *Electrochim. Acta* **2001**, *46*, 3063–3071.
(61) Wackerbarth, H.; Murgida, D. H.; Oellerich, S.; Dopner, S.; Rivas, L.; Hildebrandt, P. *J. Mol. Struct.* **2001**, *563*, 51–59.
(62) Ramirez, P.; Andreu, R.; Cuesta, A.; Calzado, C. J.; Calvente, J. J. *Anal. Chem.* **2007**, *79*, 6473–6479.

(63) Koppenol, W. H.; Rush, J. D.; Mills, J. D.; Margoliash, E. *Mol. Biol. Evol.* **1991**, *8*, 545–558.
(64) Murgida, D. H.; Hildebrandt, P. *J. Phys. Chem. B* **2001**, *105*, 1578–1586.
(65) Smith, C. P.; White, H. S. *Anal. Chem.* **1992**, *64*, 2398–2405.
(66) Wisitruangsakul, N.; Zebger, I.; Ly, H. K.; Murgida, D. H.; Ekgasit, S.; Hildebrandt, P. *Phys. Chem. Chem. Phys.* **2008**, *34*, 5276–5286.
(67) Iwata, S.; Ostermeier, C.; Ludwig, B.; Michel, H. *Nature* **1995**, *376*, 660–669.
(68) Lange, C.; Hunte, C. *Proc. Natl. Acad. Sci. U.S.A.* **2002**, *99*, 2800–2805.
(69) Pelletier, H.; Kraut, J. *Science* **1992**, *258*, 1748–1755.

JP8062383